ORIGINAL PAPER

Reaction Mechanisms and Plasma-Catalyst Interaction in Plasma-Assisted Oxidation of n-Butane: A Data-Driven Approach

D. Reiser[1] · A. von Keudell[2]

Abstract

Experimental investigations of n-butane oxidation under atmospheric-pressure plasma conditions and in He-dilution have provided detailed information on the power-dependence of the conversion of C_4H_{10} into CO and CO_2 at 450 K surface temperature. The rf-plasma discharge has been equipped with a MnO_2-catalyst, and a significant impact on the reaction chain due to the presence of the catalyst surface could be observed. We report on ongoing data-based model development. Recently, a reaction kinetic model has been published, which agrees well with the experimental data (Stewig et al. in Plasma Sources Sci Technol 32:105006, 2023). However, that model could not clearly identify the main mechanisms in the interaction of plasma and catalyst. We show that various models can be found that explain the data similarly well. Detailed sensitivity analysis shows that only a maximum of three parameters can be identified in all the models considered for the currently limited data. Despite this limitation, we intend to continue the data analysis using more general models and introduce possible surface effects. Such unified models simultaneously describe the experimental data from both measurements with and without catalyst using a single set of physical parameters. To evaluate the hypotheses, we present numerical results for certain ranges of experimental parameters, which, in a subsequent experimental verification, allows to exclude or confirm one or another model.

Introduction

Removing volatile organic compounds (VOC) from gas streams is an essential environmental technology. VOC are removed by thermal or plasma treatment, with the latter being more energy efficient and flexible [2–5]. The efficiency of the various VOC removal processes

✉ D. Reiser
  d.reiser@fz-juelich.de

[1] Institut für Energie- und Klimaforschung – Plasmaphysik, Partner of the Trilateral Euregio Cluster (TEC), Forschungszentrum Jülich GmbH, 52425 Jülich, Germany

[2] Experimentalphysik II - Reaktive Plasmen, Ruhr-Universität Bochum, 44780 Bochum, Germany

is usually validated by regarding the conversion of the VOC n-butane into CO_2 and H_2O as a benchmark reaction. In recent years [6, 7], dielectric barrier discharges (DBD) have been developed to realize such VOC removal, as this flexible and energy-efficient process can even treat large gas volumes. In addition, these DBDs are combined with a catalyst surface post plasma to assure a selectivity of the process towards CO_2 and to reduce the contribution of CO in the exhaust. Understanding the reaction mechanisms in such plasma catalysis devices is, however, extremely challenging since the multitude of possible excited species in a plasma may interact with a catalyst surface in an unknown manner. Therefore, a combined approach of experiment and modelling is often used to identify specific reaction pathways [8, 9]. This identification is not straightforward and is most often based on volume-integrated information since the typical experiment is a packed bed reactor, where the reaction products in the exhaust are being quantified combined with a global chemical model of the plasma process, invoking hundreds of species and thousands of reactions. However, in most cases, the size and complexity of such models are also associated with many uncertainties in the details (rate coefficients) of the processes considered. In addition, this always results in the risk of overparameterization if attempts are made to verify extensive models with only a few experimental data.

In this work, we want to take a principally different approach. Instead of trying to perform a forward calculation with many complex reaction chains and then comparing these with the experimental results, we want to gradually extend a data-driven model that initially gets by with only a few effective reaction mechanisms, whose rate coefficients result completely from a model regression concerning the experimental findings. The data-based model considered in this work deals exclusively with the microkinetics of gas-phase and gas-phase catalyst reactions. Details of the flow characteristics and heat transport are not considered initially. To facilitate this reduction of the models, the chemistry in the experiments is simplified by using helium dilution and a homogeneous rf discharge instead of a DBD.

Actually, our analysis aims at the identification of a reaction kinetic model of the form

$$\sum_{s=1}^{M_s} v'_{s,r} \, X_s \ \xrightarrow{\ k_r\ } \ \sum_{s=1}^{M_s} v''_{s,r} \, X_s \tag{1}$$
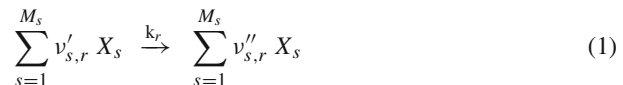
in the framework of a plug flow. Here, the integers $v'_{s,r}$ and $v''_{s,r}$ prescribe the stoichiometry and k_r are the rate coefficients for reactions labeled by $r = 1, \ldots, M_r$. With the help of experimental data for at least a few of a number of M_s species involved and plausible ideas about M_r possible reaction mechanisms, it will be investigated which microkinetic processes are relevant, whether this provides a satisfactory explanation for the observations and what the concrete reaction rates k_r are. The details of this procedure form the bulk of this text.

As a test reaction for such an approach, we analyse the oxidation of n-butane diluted in a helium rf discharge. This helium dilution assures thermal management of the molecules and reduces the impact of secondary reactions such as plasma polymerization.

The data from this experiment, the details of which are discussed in the next section, have already been mentioned in Ref. [1] and have been compared with a reaction kinetic model for gas phase reactions. The model presented there is successful in data regression and provides first insights into possible reaction mechanisms involved in the plasma catalytic conversion of n-butane. Nevertheless, there are some unresolved issues: (1) the model is overparameterized, and a variety of models can perform similarly good regression, (2) the rate coefficients obtained in the regression differ significantly in some cases from known literature values, and—most importantly—(3) no surface model has been included, and the data for experiments with and without catalyst are analyzed separately, allowing only vague

speculations about the physical effects of the catalyst. Here, we want to extend this data analysis and discuss the details of the issues mentioned. It is shown that

- The current experimental findings do not allow the determination of more than three reaction kinetic parameters. All more complex models with a larger number of parameters provide large uncertainties and many possible parameter combinations. The problem of overparameterization is primarily due to the lack of information on oxygen kinetics.
- The consideration of surface effects, discussed in other work, allows the gas-phase chemistry to be unified and provides a consistent model regression for all experimental data simultaneously.

It should be noted that surface models add considerable value to the model by avoiding speculation about the relationship between two different regressions. However, since even these model extensions cannot be unambiguously verified from the current data, predictions for future experiments are shown to help evaluate and choose between models. This will be the important aspect in Sect. 7. Beyond this specific example—the conversion of n-butane—we also want to document in this paper the general approach of our data-driven model regression, which is specifically based on the concrete information of the experiment in order to avoid possible overparameterization of models. This method will also be used for other experimental studies in the future and will therefore be described in detail.

Experiment

The experiments formed in a well-defined plasma channel, where a plasma slab of 1 mm $\times$ 13 mm $\times$ 26 mm is created by plane parallel electrodes. The electrodes are covered by glass plates, forming a gap of 1 mm. An rf plasma is ignited in this gap in a gas mixture of helium and a 1% admixture of a stoichiometric combination of n-butane and oxygen. For this, the helium flow is set to 250 sccm to which 0.31 sccm n-butane and 2.03 sccm O_2 are added for a complete conversion of n-butane into CO_2 and H_2O. The absorbed power is measured via a VI probe in the feed lines of the RF plasma. The catalyst is MnO_2 sprayed on the glass plates with a loading of 3 mg/cm^2. The complete setup is heated to 450 K. The plasma conversion is measured using infrared spectroscopy to measure the absorbance of the different species in the central part of the plasma channel. By modeling the absorption spectra based on the HiTRAN database, the rotational and vibrational temperatures are determined to be close to 450 K. The measured absorbance is converted into concentration based on known line strengths. The experimental data thus yield the concentrations of C_4H_{10}, CO_2 and CO for different plasma powers, and the data were acquired for discharges with and without a catalyst. Further details of the experiment are described in [10, 11].

Problem Statement: Reaction Kinetics Simulation

The situation to be considered is the following. A gas flow goes through the discharge region and is in touch with a catalyst surface where certain surface species are present. It is assumed that all gas species are moving with a constant velocity v and that the surface is stationary and stable. Therefore, no surface modification processes have to be taken into account and the entire system is assumed to be in a stationary state. In Fig. 1 a sketch is shown to depict the experiment: the inflow of the gas is controlled at $x = 0$ and the measurements are done
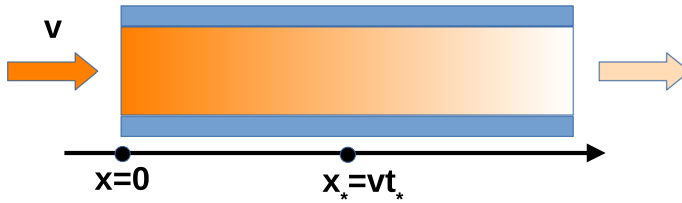
Fig. 1 Sketch of the experimentally prepared 1d-flow of gas in the plasma chamber

at a position $x_* = vt_*$, where t_* is the residence time of the gas species between $x = 0$ and $x = x_*$.

The system of reaction kinetic equations for constant 1D flow in x-direction can be written as

$$\frac{dN_i(x,t)}{dt} + v_i \frac{dN_i(x,t)}{dx} = R_i(x,t) \tag{2}$$

Here $i = 1, \ldots, M$ is the species index and N_i the corresponding species density. The respective flow speeds and reaction terms are denoted by v_i and R_i, respectively. If $dN_i/dt = 0$ and the corresponding flow velocity v_i is finite this results in

$$v_i \frac{dN_i(x)}{dx} = R_i(x) \tag{3}$$

This is the form of rate laws for the gas phase species. For the immobile surface species one obtains $R_i(x) = 0$ for the corresponding surface reactions. The general form of the reaction terms R_i is described in "Appendix A". There, the calculation of sensitivities is also explained, which is related and needed for the later statistical analysis. Note that the discussion in Ref. [1] used rate equations describing time-varying processes. This was possible because only gas particles were considered, which allows a simple transformation to a co-moving coordinate system. Like in that report, the task is to find suitable reaction terms for different plasma powers that reproduce measured species densities for given initial conditions at $x = 0$ when integrating from $x = 0$ to $x_* = vt_*$.

## Preliminaries: Simple Data Regression

Before we discuss physically plausible models, we would first like to address some of the purely mathematical peculiarities of the measured data. It is found that the dependence of the species densities $N_{C_4H_{10}}$, N_{CO} and N_{CO_2} observed at the measuring point on the plasma power P can be accurately described by a straightforward set of linear differential equations.

$$\frac{dN_{C_4H_{10}}}{dP} = -c_1 \, N_{C_4H_{10}} \tag{4}$$

$$\frac{dN_{CO}}{dP} = 4c_1 \, N_{C_4H_{10}} - c_2 \, N_{CO} + c_3 \, N_{CO_2} \tag{5}$$

$$\frac{dN_{CO_2}}{dP} = c_2 \, N_{CO} - c_3 \, N_{CO_2} \tag{6}$$

where $c_1 = c_1(x)$, $c_2 = c_2(x)$ and $c_3 = c_3(x)$ are functions of x but independent of P. This set of equations even has an analytical solution. The results are shown in Fig. 2 and are of astonishing quality.
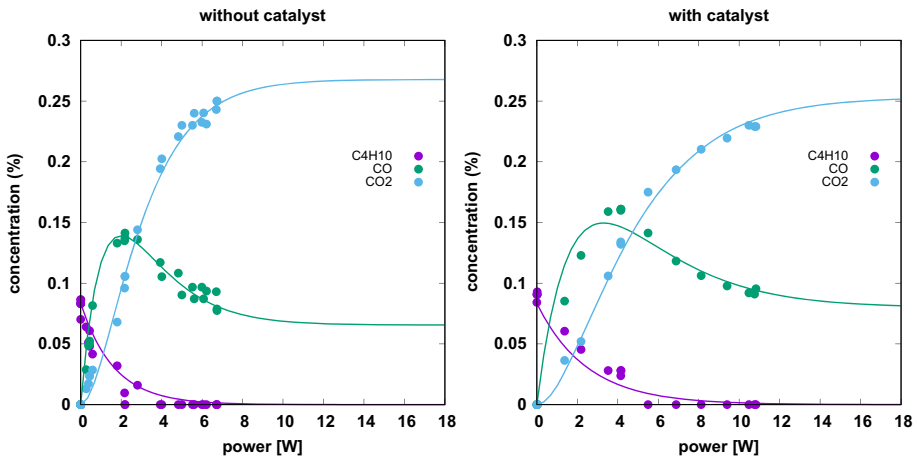
Fig. 2 Comparison of the experimental data with the results of the model defined by Eqs. 4–6. The regression parameters at the measurement point x_* are $c_1(x_*) = 0.608\,\text{W}^{-1}$, $c_2(x_*) = 0.516\,\text{W}^{-1}$ and $c_3(x_*) = 0.125\,\text{W}^{-1}$ for the case without catalyst and $c_1(x_*) = 0.403\,\text{W}^{-1}$, $c_2(x_*) = 0.297\,\text{W}^{-1}$ and $c_3(x_*) = 0.0939\,\text{W}^{-1}$ for the case with catalyst

The excellent description of the experimental data is therefore considered a validated result. In a next step of analysis one could try to derive a set of differential equations for the dependence of the densities on x from these equations. Indeed, the simple structure of the solutions makes it possible to find a representation of the linear form

$$\frac{dN_i}{dx} = \sum_{j=1}^{3} \frac{dN_i}{dc_j} \cdot \frac{dc_j}{dx} \equiv \sum_j H_{ij} N_j \tag{7}$$

Nevertheless, this re-formulation does not lead any further because the information about the spatial dependence of $c_1(x)$, $c_2(x)$ and $c_3(x)$ is missing, and an interpretation in terms of reaction mechanisms providing the rhs of Eq. 3 is not unique.

Despite all this, this simple regression using only three parameters provides important insight into the sensitivity analysis of other—perhaps more complex—models. If one assumes, that the coefficients c_j depend on some other parameters $k_l, l = 1, \ldots, L, L > 3$, one obtains for a particular density N_i at a particular plasma power P that

$$\frac{dN_i}{dk_l} = \sum_{j=1}^{3} \frac{\partial N_i}{\partial c_j} \frac{dc_j}{dk_l} \tag{8}$$

Considering now a vector $\mathbf{N}$ containing M densities computed by a particular model for different plasma powers prescribed by the experiment, the sensitivity matrices with respect to the model parameters $\mathbf{k}$ and $\mathbf{c}$ are given as

$$\mathbf{S} = \left(\frac{d\mathbf{N}}{d\mathbf{k}}\right)^{\text{T}} \cdot \frac{d\mathbf{N}}{d\mathbf{k}} \quad , \quad \mathbf{S}' = \left(\frac{d\mathbf{N}}{d\mathbf{c}}\right)^{\text{T}} \cdot \frac{d\mathbf{N}}{d\mathbf{c}} \tag{9}$$

For sensitivity analysis details, see "Appendices B and C". Here $d\mathbf{N}/d\mathbf{k} \in \mathbb{R}^{M \times L}$, $d\mathbf{N}/d\mathbf{c} \in \mathbb{R}^{M \times 3}$ and $d\mathbf{c}/d\mathbf{k} \in \mathbb{R}^{3 \times L}$ and due to the relations

$$\mathbf{S} = \left(\frac{d\mathbf{c}}{d\mathbf{k}}\right)^{\mathrm{T}} \cdot \mathbf{S}' \cdot \frac{d\mathbf{c}}{d\mathbf{k}}, \quad \mathrm{rank}\,\frac{d\mathbf{c}}{d\mathbf{k}} \leq 3, \quad \mathrm{rank}\,\mathbf{S}' \leq 3 \tag{10}$$

it follows that

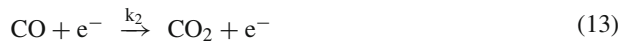$$\mathrm{rank}\,\mathbf{S} \leq 3 \tag{11}$$

This result can be summarized as follows: if the simple model with three parameters works well—and it does indeed—the introduction of a more complex model with $L > 3$ parameters gives a singular sensitivity matrix with a maximum rank of three. Then a maximum of only three parameters can be identified and the model is overparameterized. This result will be quoted in the next sections several times and is important because it explains the ambiguities in model finding.

Regression with Gas Phase Plasma Models

In this section, we first examine gas-phase models that perform separate regressions of the experimental findings for the cases with and without catalysts. This corresponds to the discussion in Ref. [1] where the concrete physics of the plasma-surface interaction is not considered. The same model for reactions in the gas phase is assumed for both cases, but with different rate coefficients. Here, an optimization procedure based on a genetic algorithm is used to determine the optimal rate coefficients of the reaction kinetic model. The goal of the optimization is to obtain a good agreement between the experimental data taken at the measurement point $x = x_*$ and the results of rate law integration between $x = 0$ and x_* for all values of plasma power P considered in the experiment. For details see "Appendix B" and Ref. [12]. Sensitivity analysis and confidence intervals provide information on the quality of the model regressions. The results are compared with the model from Ref. [1].

Reference Model with Three Gas Phase Processes

A very simple microkinetic model can be set up to obtain the relations Eqs. 4–6 by assuming conversion processes of the form

$$C_4H_{10} + e^- \xrightarrow{k_1} 4CO + e^- \tag{12}$$

$$CO + e^- \xrightarrow{k_2} CO_2 + e^- \tag{13}$$

$$CO_2 + e^- \xrightarrow{k_3} CO + e^- \tag{14}$$

All processes involve the participation of electrons, and the rate coefficients k_i, $i = 1, \ldots, 3$ are assumed to be constant. Then, the rate laws read as

$$v\,\frac{dN_{C_4H_{10}}}{dx} = -k_1\,N_{C_4H_{10}}\,N_{e^-} \tag{15}$$

$$v\,\frac{dN_{CO}}{dx} = 4\,k_1\,N_{C_4H_{10}}\,N_{e^-} - k_2\,N_{CO}\,N_{e^-}$$
$$+k_3\,N_{CO_2}\,N_{e^-} \tag{16}$$

Table 1 Optimal values (MLE) for the model parameters $\hat{k}_1$, $\hat{k}_2$ and $\hat{k}_3$ given in units $10^{-16}\,\mathrm{m}^3/s$

Parameter		MLE	Confidence
	$\hat{k}_1$	1.114	[0.979: 1.268]
(wo cat)	$\hat{k}_2$	0.946	[0.787: 1.138]
	$\hat{k}_3$	0.231	[0.142: 0.378]
	$\hat{k}_1$	0.730	[0.619: 0.862]
(w cat)	$\hat{k}_2$	0.544	[0.445: 0.666]
	$\hat{k}_3$	0.172	[0.109: 0.271]

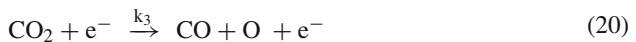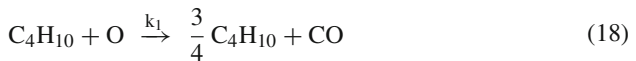$$v\,\frac{dN_{CO_2}}{dx} = k_2\,N_{CO}\,N_{e^-} - k_3\,N_{CO_2}\,N_{e^-} \tag{17}$$

The electron density is assumed to be a linear function of plasma power P, i.e. $N_{e^-} = \alpha\,P$ and the flow speed $v = $ const. is the same for all gas phase species. These equations also have an analytical solution identical to the solution of the reference Eqs. 4–6 when $c_i(x_*) = \alpha k_i t_*$. Therefore, this model reproduces the results of Fig. 2. Using $\alpha = 1.25 \times 10^{17}\,\mathrm{m}^{-3}\mathrm{W}^{-1}$ and $t_* = 4.37 \times 10^{-2}\,$s to reflect the experimental conditions, one finds rate coefficients listed as in Table 1. They have been found by a Maximum Likelihood Estimate (MLE) as explained in "Appendix B".

Confidence intervals are computed according to the recipe also described in "Appendix B". As expected from the discussion in Sect. 4 the three parameters $\hat{k}_1$, $\hat{k}_2$ and $\hat{k}_3$ lead to a full rank three sensitivity matrix. The confidence intervals are relatively narrow and constrain the order of magnitude quite precisely. This means that the information about all assumed processes contained in the data is sufficient to determine the rate coefficients fairly precisely. However, the model gives balance equations rather than a detailed description of physical processes. Models based on concrete plasma chemical reactions are presented in the next sections.

Reaction Kinetic Model with Five Gas Phase Reactions

The basic model of the last section works very well, but just like the reference model of Sect. 4, it is rather a mathematical description reflecting the basic properties of the data situation. Now reasonable physical processes are to be considered, which give a plausible explanation for the experimental findings. For this purpose, we recapitulate briefly the model from Ref. [1]:

$$C_4H_{10} + O \xrightarrow{k_1} \frac{3}{4}\,C_4H_{10} + CO \tag{18}$$

$$CO + O + He \xrightarrow{k_2} CO_2 + He \tag{19}$$

$$CO_2 + e^- \xrightarrow{k_3} CO + O + e^- \tag{20}$$

$$O_2 + e^- \xrightarrow{k_4} O + O + e^- \tag{21}$$

$$O + O + He \xrightarrow{k_5} O_2 + He \tag{22}$$

with rate laws given by

$$v\,\frac{\partial N_{C_4H_{10}}}{\partial x} = -\frac{k_1}{4}\,N_{C_4H_{10}}\,N_O \tag{23}$$
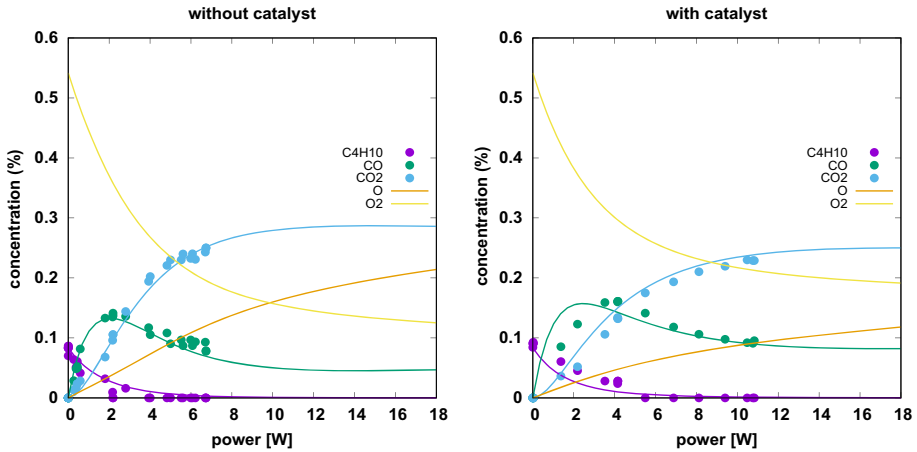
Fig. 3 Comparison of the experimental data with the results of the model defined by Eqs. 23–27. The rate coefficients are listed in Table 2 and are taken from Ref. [1]

$$v \frac{\partial N_{\text{CO}}}{\partial x} = k_1 N_{\text{C}_4\text{H}_{10}} N_\text{O} - k_2 N_{\text{CO}} N_\text{O} N_{\text{He}}$$

$$+ k_3 N_{\text{CO}_2} N_{\text{e}^-} \tag{24}$$

$$v \frac{\partial N_{\text{CO}_2}}{\partial x} = k_2 N_{\text{CO}} N_\text{O} N_{\text{He}} - k_3 N_{\text{CO}_2} N_{\text{e}^-} \tag{25}$$

$$v \frac{\partial N_\text{O}}{\partial x} = -k_1 N_{\text{C}_4\text{H}_{10}} N_\text{O} - k_2 N_{\text{CO}} N_\text{O} N_{\text{He}}$$
$$+ k_3 N_{\text{CO}_2} N_{\text{e}^-} + 2 k_4 N_{\text{O}_2} N_{\text{e}^-} - 2 k_5 N_\text{O}^2 N_{\text{He}} \tag{26}$$

$$v \frac{\partial N_{\text{O}_2}}{\partial x} = -k_4 N_{\text{O}_2} N_{\text{e}^-} + k_5 N_\text{O}^2 N_{\text{He}} \tag{27}$$

Again $\alpha = 1.25 \times 10^{17}\,\text{m}^{-3}\text{W}^{-1}$, $t_* = 4.37 \times 10^{-2}\,\text{s}$ and also $N_{\text{He}} = 2.4 \times 10^{25}\,\text{m}^{-3}$ are used as prescribed by the experimental conditions. In Table 2 we recall the rate coefficients proposed in Ref. [1] and for a clear discussion, we also relate the rate coefficients to the same reference values given there: $k_{1,\text{ref}} = 5.0 \times 10^{-22}\,\text{m}^3/\text{s}$, $k_{2,\text{ref}} = 1.2 \times 10^{-46}\,\text{m}^6/\text{s}$, $k_{3,\text{ref}} = 1.0 \times 10^{-17}\,\text{m}^3/\text{s}$, $k_{4,\text{ref}} = 3.7 \times 10^{-17}\,\text{m}^3/\text{s}$ and $k_{5,\text{ref}} = 2.53 \times 10^{-46}\,\text{m}^6/\text{s}$. We show the fit curves resulting from this particular choice of rate coefficients in Fig. 3.

As discussed in Ref. [1], the fit curves show relatively good agreement with the measured concentrations. Here, we go a step beyond this and use these results as a starting point for optimization using the genetic algorithm, i.e. the model parameters are optimized using the rate coefficients from Table 2 as starting guess. The results of the optimization are listed in Table 3 and Fig. 4 shows the corresponding fit curves. It can be seen from Figs. 3 and 4 that the optimization improves the regression quality, particularly for the case with catalyst. Also, the confidence intervals of the optimized rate coefficients in Table 3 are significantly smaller than the ones in Table 2. However, it should be noted that the optimization leads to the conclusion that the process $\text{O} + \text{O} + \text{He} \xrightarrow{k_5} \text{O}_2 + \text{He}$ can be viewed as negligible for the case without a catalyst. This result does not seem physically plausible. On the other hand, also the reaction $\text{C}_4\text{H}_{10} + \text{O} \xrightarrow{k_1} \frac{3}{4}\,\text{C}_4\text{H}_{10} + \text{CO}$ is only an approximation for a large number of processes involving oxygen, so that a discrepancy to a certain recombination process

Table 2 Proposed values for the model parameters $\hat{k}_1$–$\hat{k}_5$ from Ref. [1]

| Parameter		Ref. [1]	Confidence
	$\hat{k}_1/k_{1,\mathrm{ref}}$	26.00	$[1.38 \times 10^0 : 4.89 \times 10^2]$
	$\hat{k}_2/k_{2,\mathrm{ref}}$	1.00	$[6.89 \times 10^{-2} : 1.45 \times 10^1]$
(wo cat)	$\hat{k}_3/k_{3,\mathrm{ref}}$	1.00	$[7.30 \times 10^{-3} : 1.37 \times 10^2]$
	$\hat{k}_4/k_{4,\mathrm{ref}}$	1.00	$[3.90 \times 10^{-2} : 2.55 \times 10^1]$
	$\hat{k}_5/k_{5,\mathrm{ref}}$	0.15	$[1.23 \times 10^{-6} : 1.82 \times 10^4]$
	$\hat{k}_1/k_{1,\mathrm{ref}}$	38.00	$[3.10 \times 10^{-2} : 4.65 \times 10^4]$
	$\hat{k}_2/k_{2,\mathrm{ref}}$	1.00	$[1.28 \times 10^{-3} : 7.78 \times 10^2]$
(w cat)	$\hat{k}_3/k_{3,\mathrm{ref}}$	1.00	$[1.95 \times 10^{-3} : 5.11 \times 10^2]$
	$\hat{k}_4/k_{4,\mathrm{ref}}$	1.00	$[2.33 \times 10^{-4} : 4.27 \times 10^3]$
	$\hat{k}_5/k_{5,\mathrm{ref}}$	0.75	$[2.11 \times 10^{-10} : 2.66 \times 10^9]$

Reference values $k_{i,\mathrm{ref}}$ are given in the text

Table 3 Optimized values (MLE) for the model parameters $\hat{k}_1$–$\hat{k}_5$

Parameter		MLE	Confidence
	$\hat{k}_1/k_{1,\mathrm{ref}}$	20.00	$[7.52 \times 10^0 : 5.32 \times 10^1]$
	$\hat{k}_2/k_{2,\mathrm{ref}}$	0.82	$[2.49 \times 10^{-1} : 2.71 \times 10^0]$
(wo cat)	$\hat{k}_3/k_{3,\mathrm{ref}}$	4.56	$[1.56 \times 10^0 : 1.33 \times 10^1]$
	$\hat{k}_4/k_{4,\mathrm{ref}}$	1.09	$[4.42 \times 10^{-1} : 2.69 \times 10^0]$
	$\hat{k}_5/k_{5,\mathrm{ref}}$	0.0	$[0.0 : 0.0]$
	$\hat{k}_1/k_{1,\mathrm{ref}}$	24.67	$[5.09 \times 10^0 : 1.19 \times 10^2]$
	$\hat{k}_2/k_{2,\mathrm{ref}}$	0.82	$[1.19 \times 10^{-1} : 6.00 \times 10^0]$
(w cat)	$\hat{k}_3/k_{3,\mathrm{ref}}$	3.06	$[4.49 \times 10^{-1} : 2.08 \times 10^1]$
	$\hat{k}_4/k_{4,\mathrm{ref}}$	0.63	$[0.63 \times 10^{-1} : 3.06 \times 10^0]$
	$\hat{k}_5/k_{5,\mathrm{ref}}$	0.0	$[0.0 : 0.0]$

Reference values $k_{i,\mathrm{ref}}$ are given in the text

can also occur. The most critical point when considering the two sets of rate coefficients, however, is that there is effectively a rank three sensitivity matrix in both cases. The criterion for this conclusion is that the ratios between the two smallest singular values and the largest singular value are much less than 10^{-3}, an empirical measure which has been proven useful in sensitivity analysis. As mentioned, not all five rate coefficients can be determined accurately using the available data and—to complicate matters further—numerical experiments have shown that there are a variety of combinations of rate coefficients that produce similarly good regressions (for C_4H_{10}, CO, and CO_2), and other processes than the oxygen recombination may appear to be negligible. It turns out that the model development suffers from the lack of oxygen data. A similar problem appeared in the analysis of methane conversion in Ref. [12]. An investigation of Lie transformations shows that the model Eqs. 23–27 allow an infinite number of combinations of rate coefficients and provide good regression as long as the oxygen concentrations N_O and N_{O_2} can be set arbitrarily and are not limited by experimental data. Actually, one can see that the results for oxygen shown in Figs. 3 and 4 are very different, even though both models reproduce the experimental data for C_4H_{10}, CO, and CO_2 very well. We do not want to go into this discussion any further. Given the data available, we want
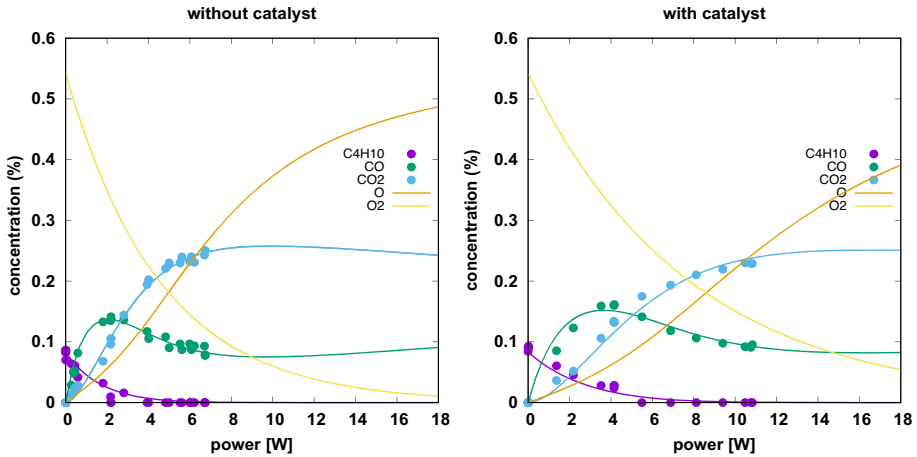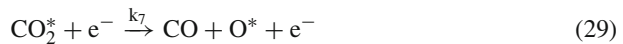
Fig. 4 Comparison of the experimental data with the results of the model defined by Eqs. 23–27. The rate coefficients are listed in Table 3 and are obtained by an optimization using the rate coefficients of Table 2 as starting guess

to emphasize that there is currently no way to assess the quality of the model parameters in Tables 2 and 3 or other variants without additional information on oxygen concentrations. Despite this limitation, an attempt should at least be made to close the gap between the regressions found separately for the data with and without catalyst. This is the content of the next sections, where also possibilities of comparing different models experimentally, even without measuring oxygen concentrations, are discussed.

Regression with Plasma-Catalyst Models

We now turn to an extension of the reaction scheme described by Eqs. 18–22 introducing even more model parameters. Two models for surface processes will be discussed. Both are based on ideas from previous work investigating the interaction of CO, CO_2, O and O_2 with catalytic surfaces. We limit ourselves to extensions through three reactions and consider what we denote Surface Model I and Surface Model II in detail. In these models, the asterisk labels surface species, e. g. "O*" denotes adsorbed atomic oxygen and the species "*" labels a free surface site.

(1) Surface Model I:

$$CO_2 + * \xrightarrow{k_6} CO_2^* \tag{28}$$

$$CO_2^* + e^- \xrightarrow{k_7} CO + O^* + e^- \tag{29}$$

$$O + O^* \xrightarrow{k_8} O_2 + * \tag{30}$$

The overall reaction for the gas species is $CO_2 + O + e^- \rightarrow CO + O_2 + e^-$ and the rate laws are

$$v \frac{dN_{CO}}{dx} = k_7 N_{CO_2^*} N_{e^-} \tag{31}$$

$$v \, \frac{dN_{CO_2}}{dx} = -k_6 \, N_{CO_2} \, N_* \tag{32}$$

$$v \, \frac{dN_O}{dx} = -k_8 \, N_O \, N_{O^*} \tag{33}$$

$$v \, \frac{dN_{O_2}}{dx} = k_8 \, N_O \, N_{O^*} \tag{34}$$

$$v \, \frac{dN_{CO_2^*}}{dx} = k_6 \, N_{CO_2} \, N_* - k_7 \, N_{CO_2^*} \, N_{e^-} \tag{35}$$

$$v \, \frac{dN_{O^*}}{dx} = k_7 \, N_{CO_2^*} \, N_{e^-} - k_8 \, N_O \, N_{O^*} \tag{36}$$

The density of free surface sites N_* is given by the conservation law $N_* + N_{CO_2^*} + N_{O^*} = \Gamma A/V$, where Γ denotes the surface site density, A the active area of the catalyst and V the volume of the plasma chamber.

This is a reaction mechanism inspired by the work of Chen [13], where the impact of metal oxide surfaces on CO_2 conversion has been investigated. A CO_2 molecule is split by dissociative electron attachment after being adsorbed at the surface. A healing mechanism fills the oxygen vacancy by an Eley–Rideal type process.

As mentioned in Sect. 3 the surface species are assumed to be immobile, and the surface is expected to be in a stationary (saturated) state, i.e. we will not consider processes of surface modification that might take place in the first phase of the experiment. This is justified by the observation that the experimental data do not change even when the discharge runs for several minutes or hours. The catalyst in these experiments is probably in a self-healing state and does not change its composition. Therefore, the corresponding balance equations (stationary rate laws) for the surface species are found by setting the flow speed to zero in Eqs. 35–36 for Surface Model I. Together with the conservation law for the surface species, this gives algebraic equations for their densities as functions of the gas phase species densities, and this in turn provides sources and sinks for the gas phase rate laws. In detail, the following results

$$v \, \frac{dN_{CO}}{dx} = -v \, \frac{dN_{CO_2}}{dx} = -v \, \frac{dN_O}{dx} = v \, \frac{dN_{O_2}}{dx}$$

$$= \frac{\Gamma A}{V} \left(\frac{1}{k_8 N_O} + \frac{1}{k_6 N_{CO_2}} + \frac{1}{k_7 N_{e^-}} \right)^{-1} \tag{37}$$

The production of CO and O_2 corresponds to a destruction of CO_2 and O by the same rate of change.

The results of the optimization procedure to find the best fit rate coefficients $\hat{k}_1$–$\hat{k}_8$ are listed in Table 4 and the corresponding fit curves are shown in Fig. 5. In the regression $\Gamma = 1.6 \times 10^{19} \, \mathrm{m}^{-2}$ has been assumed for the concentration of free sites and the geometry factor is given by $A/V = 1000 \, \mathrm{m}^{-1}$. As for the previously discussed gas-phase models, the fit curves are close to the experimental data. Significant differences to the gas phase models are found in the results for O and O_2. It is found that rate coefficients $\hat{k}_1$–$\hat{k}_5$ are quite close to the results listed in Table 3 for the case without catalyst. This seems reasonable, because one can expect that the differences in the case with the catalyst should be covered by the surface processes. The corresponding rate coefficients $\hat{k}_6$–$\hat{k}_8$ are given in units of m^3/s because no appropriate literature values are available for the surface processes. However, the

Table 4 Optimal values (MLE) for the model parameters $\hat{k}_1$–$\hat{k}_8$ in the simulations with Surface Model I

Parameter	MLE
$\hat{k}_1/k_{1,\mathrm{ref}}$	2.34×10^1
$\hat{k}_2/k_{2,\mathrm{ref}}$	1.07×10^0
$\hat{k}_3/k_{3,\mathrm{ref}}$	4.29×10^0
$\hat{k}_4/k_{4,\mathrm{ref}}$	0.96×10^0
$\hat{k}_5/k_{5,\mathrm{ref}}$	2.26×10^{-12}
$\hat{k}_6$	$1.25 \times 10^{-21}\,\mathrm{m^3/s}$
$\hat{k}_7$	$1.11 \times 10^{-3}\,\mathrm{m^3/s}$
$\hat{k}_8$	$7.45 \times 10^{-9}\,\mathrm{m^3/s}$
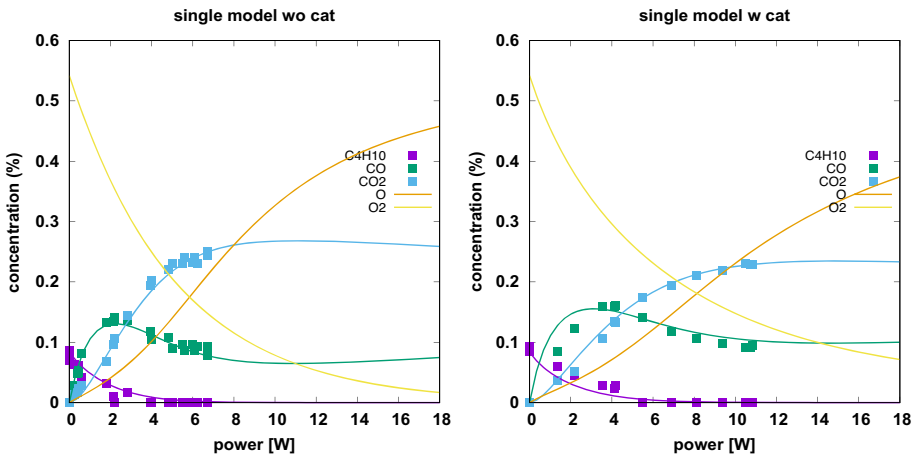
Fig. 5 Comparison of the experimental data with the results of the Surface Model I defined by Eqs. 23–27 and 31–36. The rate coefficients are listed in Table 4

rate coefficient $\hat{k}_6$ represents the adsorption of CO_2 on a MnO_2 surface. In the literature such rate coefficients are often written in the form

$$k = \frac{S_0}{\Gamma} \sqrt{\frac{RT}{2\pi M}} \qquad (38)$$

where T is the temperature in K, M is the respective molar mass in kg/mol, R is the gas constant ($R = 8.314\,\mathrm{J\,mol^{-1}\,K^{-1}}$) and S_0 is the dimensionless sticking coefficient. Inserting the respective numbers yields a sticking coefficient $S_0 = 1.7 \times 10^{-4}$. This is in the typical ranges for sticking coefficients of CO_2 on Pt and Rh known from the literature [14, 15]. Comparing the numbers for $\hat{k}_6 N_{CO_2}$, $\hat{k}_7 N_{e^-}$ and $\hat{k}_8 N_O$ in Eq. 37, one finds that the adsorption of CO_2 constitutes the rate-limiting step in the surface processes, and the additional sources and sinks in Surface Model I can be approximated by

$$v\frac{dN_{CO}}{dx} = -v\frac{dN_{CO_2}}{dx} = -v\frac{dN_O}{dx} = v\frac{dN_{O_2}}{dx}$$

$$\approx \frac{\Gamma A}{V} k_6 N_{CO_2} \qquad (39)$$

Now we turn to
(2) Surface Model II:

$$O + * \xrightarrow{k_9} O^* \tag{40}$$

$$O^* + O^* \xrightarrow{k_{10}} O_2^* + * \tag{41}$$

$$O_2^* + e^- \xrightarrow{k_{11}} O_2 + * + e^- \tag{42}$$

The overall reaction for the gas species is $O + O + e^- \rightarrow O_2 + e^-$ and the rate laws are

$$v \frac{dN_O}{dx} = -k_9 N_O N_* \tag{43}$$

$$v \frac{dN_{O_2}}{dx} = k_{11} N_{O_2^*} N_{e^-} \tag{44}$$

$$v \frac{dN_{O^*}}{dx} = k_9 N_O N_* - 2k_{10} N_{O^*}^2 \tag{45}$$

$$v \frac{dN_{O_2^*}}{dx} = k_{10} N_{O^*}^2 - k_{11} N_{O_2^*} N_{e^-} \tag{46}$$

The density of free surface sites N_* is given by the conservation law $N_* + N_{O^*} + N_{O_2^*} = \Gamma A / V$, and as before, the requirement of time-independent concentrations of surface species (flow speed zero in Eqs. 45 and 46) provides sources and sinks for the gas phase species and one obtains for Surface Model II

$$2v \frac{dN_{O_2}}{dx} = -v \frac{dN_O}{dx} = 2k_{10} N_{O^*}^2 \tag{47}$$

with N_{O^*}, the density of adsorbed atomic oxygen, determined by the quadratic equation

$$k_{10} (2k_{11}N_{e^-} + k_9 N_O) N_{O^*}^2$$
$$= (k_9 k_{11} N_O N_{e^-}) \left(\frac{\Gamma A}{V} - N_{O^*} \right) \tag{48}$$

Here, the branch is to be taken, which gives $N_{O^*} = 0$ for $\Gamma = 0$. Using this model for data regression, one obtains fit curves shown in Fig. 6 and rate coefficients listed in Table 5. Again the regression reproduces the data for C_4H_{10}, CO and CO_2 very well—with a slight improvement in the CO data, compared with the other models presented. The rate coefficients $\hat{k}_1$–$\hat{k}_3$ are about a factor 10 smaller than for Surface Model I, whereas $\hat{k}_4$ is similar. Like before, the reaction $O + O + He \xrightarrow{k_5} O_2 + He$ is not needed for the good regression. One might use Eq. 38 to estimate the sticking coefficient for O from rate coefficient $\hat{k}_9$ and this gives $S_0 = 8.54$. Of course, this value is not in accordance with the interpretation of S_0 as a probability for sticking, but it is to be emphasized that Γ is also just an estimate. Nevertheless, this estimate indicates that atomic oxygen adsorbs with a very high probability when hitting the surface. This agrees with the known high reactivity of atomic oxygen on surfaces. It follows that the coverage of O^* is about 90 % and the impact on the overall reaction mechanism is limited by the ratio $\hat{k}_{10}/\hat{k}_{11}$, i.e. the interplay of surface recombination (k_{10}) and electron induced desorption of O_2 (k_{11}).
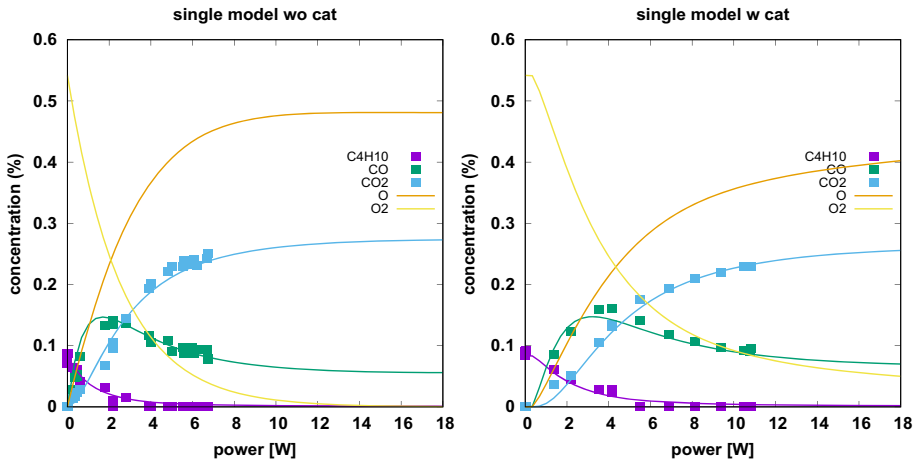
Fig. 6 Comparison of the experimental data with the results of the Surface Model II defined by Eqs. 23–27 and 43–46 The rate coefficients are listed in Table 5

Table 5 Optimal values (MLE) for the model parameters $\hat{k}_1$–$\hat{k}_5$ and $\hat{k}_9$–$\hat{k}_{11}$ in the simulations with Surface Model II

Parameter	MLE
$\hat{k}_1/k_{1,\mathrm{ref}}$	5.77×10^0
$\hat{k}_2/k_{2,\mathrm{ref}}$	1.83×10^{-1}
$\hat{k}_3/k_{3,\mathrm{ref}}$	2.00×10^{-1}
$\hat{k}_4/k_{4,\mathrm{ref}}$	1.93×10^0
$\hat{k}_5/k_{5,\mathrm{ref}}$	1.31×10^{-9}
$\hat{k}_9$	$1.03 \times 10^{-16}\,\mathrm{m^3/s}$
$\hat{k}_{10}$	$3.77 \times 10^{-21}\,\mathrm{m^3/s}$
$\hat{k}_{11}$	$4.84 \times 10^{-16}\,\mathrm{m^3/s}$

Conclusions and possibilities for model validation

Considering the results of the different models to explain the experimental data on a physical basis, it can be concluded that both the gas-phase models and the combined gas-phase-catalyst models provide satisfactory regressions. This diversity is not surprising after the remarks about overparameterization in Sect. 4. The significant differences in the predictions for oxygen densities could indicate the validity or weakness of the individual models. However, these data are not currently available. Thus, the data situation prevents us from drawing further conclusions about individual processes' relevance in the proposed reaction schemes.

However, to move the discussion forward, we would like to make suggestions at this point that open up easier access to further information in a simple way that can be realized with the current experimental possibilities. In this work, we consider two possibilities for future measurements: (1) a study of C_4H_{10} conversion with different levels of O_2 admixture, and (2) a study of CO_2 conversion without any admixture of C_4H_{10} and O_2.

We first show two examples from the variation of oxygen admixture, where all other parameters, as considered above, were left unchanged. Figure 7 shows the results for C_4H_{10}, CO and CO_2 as a function of plasma power for an initial density of $N_{O_2}(0) = 2.166\,N_{He}/100$.
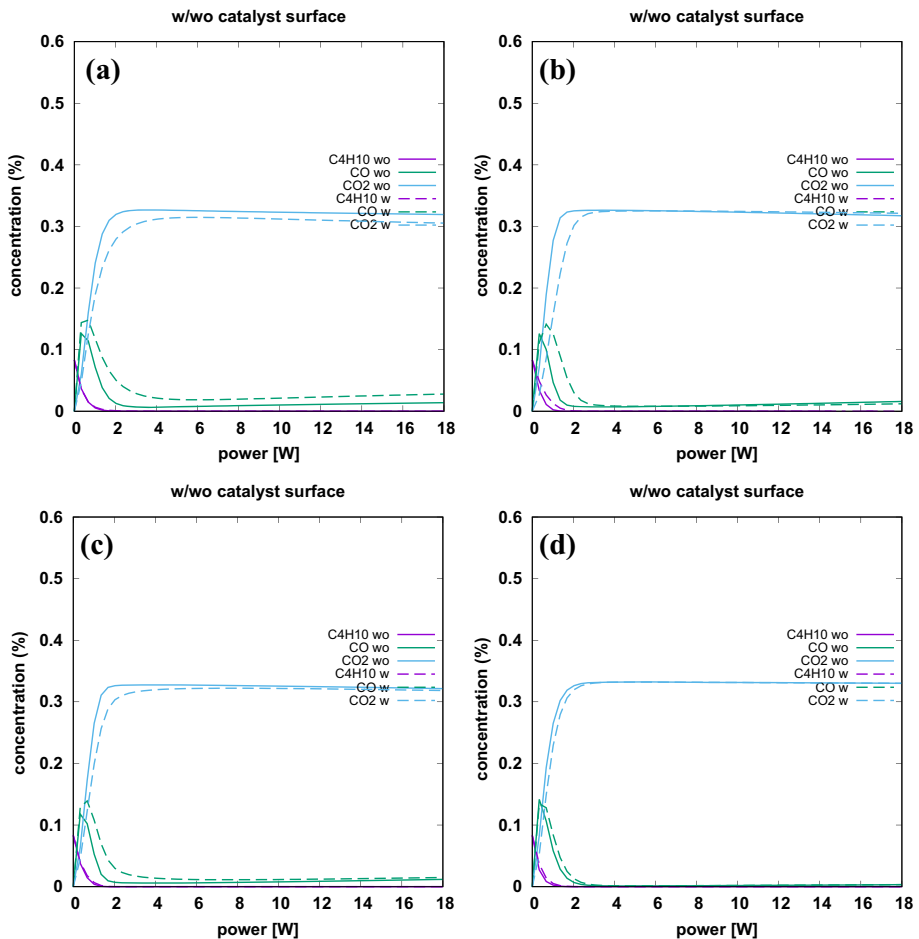
Fig. 7 Prediction of regression models for O_2 initial density of $N_{O_2}(0) = 2.166\,N_{He}/100$. The gas feed of C_4H_{10} is the same as for the regression results discussed above. **a** Gas-phase model with rate coefficients of Table 2, **b** gas-phase model with optimized rate coefficients of Table 3, **c** Surface Model I (Table 4) and **d** Surface Model II (Table 5)

The calculations were made for the model of Ref. [1] (a), the optimized model with rate coefficients listed in Table 3 (b), Surface Model I (c) and Surface Model II (d). It is remarkable that all predictions are very similar. In particular, the impact of the catalyst on the product spectrum is only small and limited to small plasma powers. Such a prediction does not help to distinguish between the different models presented. Nevertheless, it may give an indication of whether the basic features of these models can fit the reaction kinetics for other experimental conditions.

A more pronounced difference between the model predictions can be seen in Fig. 8, where the results for an initial O_2-density of $N_{O_2}(0) = 0.135\,N_{He}/100$ are shown. The models (a), (b), and (c) again look quite similar, but model (d) gives a very different result with a significant impact of the catalyst for plasma powers in the range up to 10 W. For lower values of P it seems that the presence of the catalyst inhibits the conversion of C_4H_{10} and
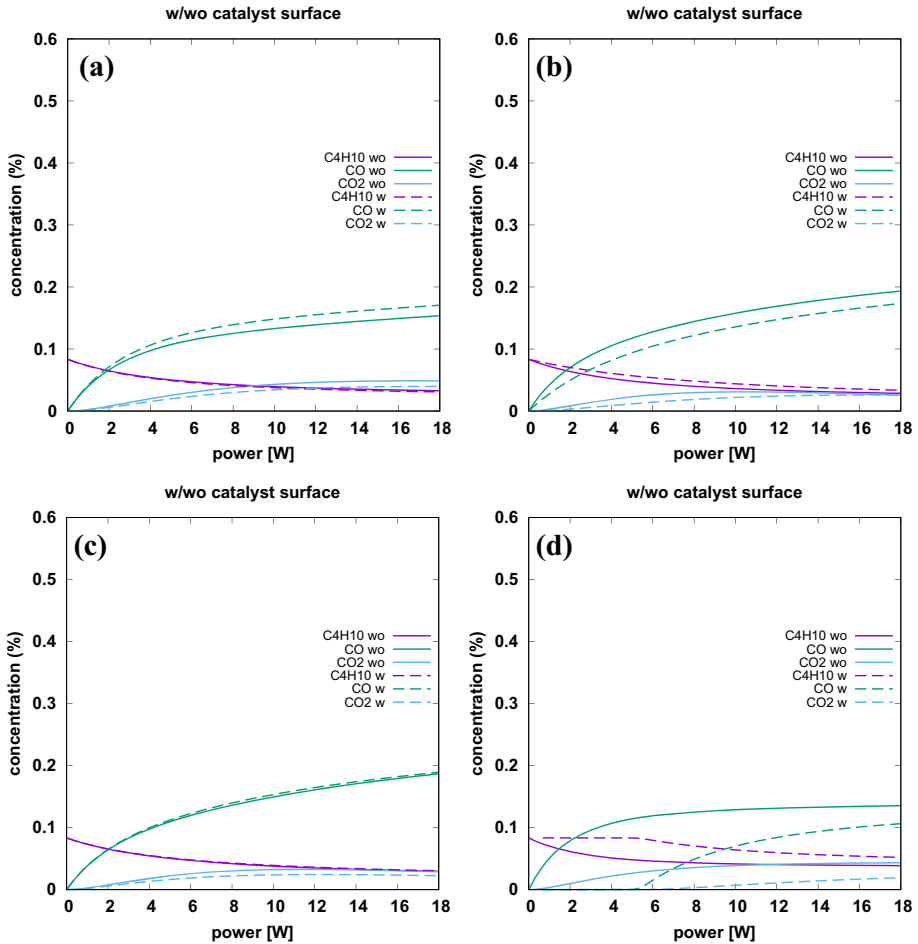
Fig. 8 Prediction of regression models for O_2 initial density of $N_{O_2}(0) = 0.135\, N_{He}/100$. The gas feed of C_4H_{10} is the same as for the regression results discussed above. **a** Gas-phase model with rate coefficients of Table 2, **b** gas-phase model with optimized rate coefficients of Table 3, **c** Surface Model I (Table 4) and **d** Surface Model II (Table 5)

that there is almost no CO at the measurement point. This result could be used to distinguish between models (a), (b), and (c) on the one hand and model (d) on the other.

Another test we want to propose considers the case where only CO_2 is added to the helium flow. The densities of C_4H_{10} and O_2 are set to zero, so that only a possible CO_2 conversion due to the presence of electrons and/or a catalytic surface is examined.

The results for a CO_2 initial density of $N_{CO_2}(0) = 2.166\, N_{He}/100$ are shown in Fig. 9. The models (a), (b), and (d) lead to very similar results and, whereas these do not show a very strong impact of the catalyst, the model (c) indicates a significant change in CO_2 conversion if the catalyst is present. This prediction can be used to decide whether CO_2 and CO are involved in surface processes.

Finally, the results for a CO_2 initial density of $N_{CO_2}(0) = 0.135\, N_{He}/100$ are presented in Fig. 10. As for the case with high CO_2-feed, the models (a), (b), and (d) show only a small
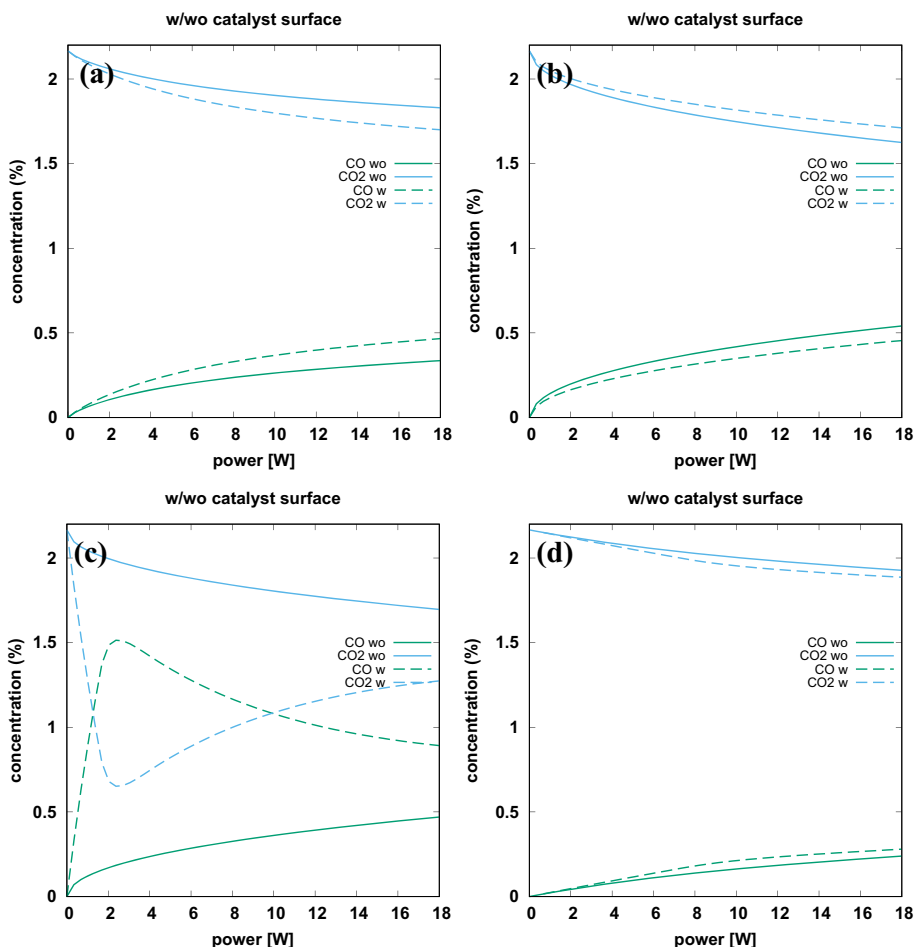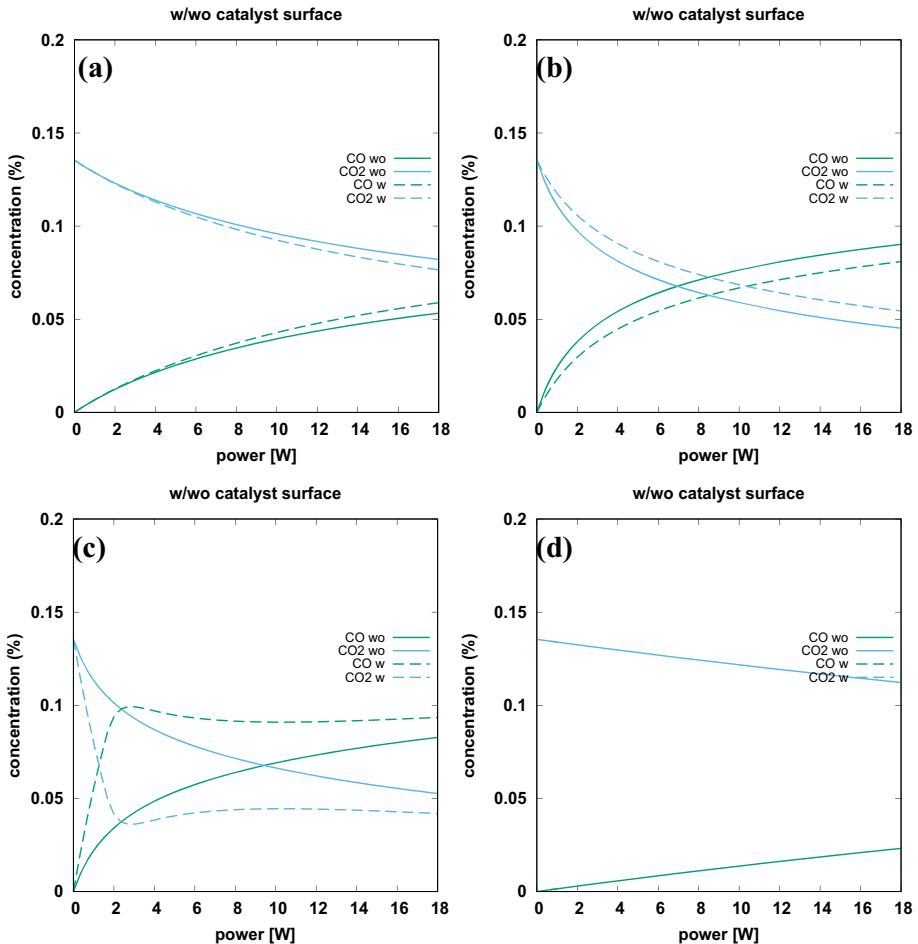
Fig. 9 Prediction of regression models for CO_2 initial density of $N_{CO_2}(0) = 2.166\, N_{He}/100$. The gas feed of C_4H_{10} and O_2 is set to zero. **a** Gas-phase model with rate coefficients of Table 2, **b** gas-phase model with optimized rate coefficients of Table 3, **c** Surface Model I (Table 4) and **d** Surface Model II (Table 5)

catalytic effect. Contrary to this, model (c) shows again a strong catalytic effect. Moreover, the power dependence of the conversion is very different in models (a), (b) and (d) and this might give a strong hint to distinguish between the underlying model assumptions (role of oxygen recombination in the gas phase and on the surface).

Summary

We examined the experimental data and the reaction kinetic model from Ref. [1] and found that the current data do not allow a clear interpretation. Detailed sensitivity analysis confirms that only three parameters can be determined with certainty. To make the modelling more realistic, surface models were proposed to extend the previous model regression approach, where the experimental data with and without catalyst were considered separately. It is

Fig. 10 Prediction of regression models for CO_2 initial density of $N_{CO_2}(0) = 0.135\,N_{He}/100$. The gas feed of C_4H_{10} and O_2 is set to zero. **a** Gas-phase model with rate coefficients of Table 2, **b** gas-phase model with optimized rate coefficients of Table 3, **c** Surface Model I (Table 4) and **d** Surface Model II (Table 5)

shown that these models can also easily describe the data and provide quite reasonable rate coefficients. This ambiguity does not allow us at the moment to clarify what role, for example, oxygen gas phase recombination or the surface processes involving oxocarbon and oxygen might play. A clear decision as to which model better describes reality needs data on oxygen concentrations, but since experiments to determine the oxygen concentration are currently only being set up or are only available for other temperatures and with considerable effort, we have made suggestions for experimental investigations that, even with simpler setups, allow us to provide information about the validity of the various models proposed. Varying the O_2 density allows us to check whether Surface Model II represents a useful extension, as its predictions for small O_2 admixtures differ significantly from the other models we have discussed. On the other hand, an experiment with a high O_2 admixture allows one to decide whether any of the models presented are useful for describing further experiments in a meaningful way, or whether other processes should be taken into account. Much stronger

evidence for or against any of the presented models comes from our numerical experiments for the case where an admixture of CO_2 without n-butane and oxygen is used. This eliminates the complex process of C_4H_{10} conversion and elementary processes of the models presented can be tested. The models provide significantly different results, which could provide information in an experimental test as to whether it makes sense to neglect oxygen recombination and whether the processes on the catalytic surface are more likely to occur via CO_2 and CO or only via O or O_2.

The methods and results presented here are intended to use numerical simulations to stimulate meaningful experiments that allow a better understanding the reaction kinetics of the interaction of plasma-gas processes with a catalytic surface.

Data Availability The data that support the findings of this study are available from the corresponding author upon reasonable request.
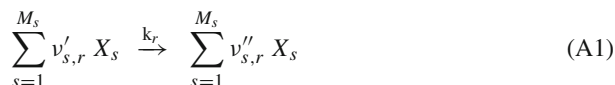
Declarations

Ethical Approval Not applicable.

Appendix A: Computation of Sensitivities

In general, the reaction kinetics for M_r reactions and M_s species can be written as

$$\sum_{s=1}^{M_s} v'_{s,r} \, X_s \; \xrightarrow{k_r} \; \sum_{s=1}^{M_s} v''_{s,r} \, X_s \tag{A1}$$

where the integers $v'_{s,r}$ and $v''_{s,r}$ prescribe the stoichiometry and k_r are the rate coefficients for reactions $r = 1, \ldots, M_r$. The corresponding rate laws for the species densities $N_s, s = 1, \ldots, M_s$ are

$$v_s \, \frac{dN_s}{dx} = \sum_{r=1}^{M_r} (v''_{s,r} - v'_{s,r}) \, k_r \prod_{p=1}^{M_s} N_p^{v'_{p,r}} \tag{A2}$$

Defining the sensitivity with respect to the rate coefficients by

$$Z_{s,l} = \frac{dN_s}{dk_l} \tag{A3}$$

the determining equation for the matrix element $Z_{s,l}$ is found as

$$
\begin{aligned}
v_s \frac{dZ_{s,l}}{dx} &= (v''_{s,l} - v'_{s,l}) \prod_{p=1}^{M_s} N_p^{v'_{p,l}} \\
&+ \sum_{r=1}^{M_r} (v''_{s,r} - v'_{s,r}) k_r \sum_{p=1}^{M_s} Z_{p,l} \, v'_{p,r} \, N_p^{-1} \prod_{k=1}^{M_s} N_k^{v'_{k,r}}
\end{aligned} \tag{A4}
$$

All species densities N_s at position $x = 0$ are determined just by the experimental setup and not by any reaction rates k_l. Therefore, $Z_{s,l} = 0$ at position $x = 0$ is used to solve the coupled system for the densities N_s and the derivatives $Z_{s,l}$.

Note that similarly, one can also compute the sensitivity cwith respect to an initial condition

$$
H_{s,l} = \frac{dN_s}{dN_l(0)} \tag{A5}
$$

which fulfils

$$
v_s \frac{dH_{s,l}}{dx} = \sum_{r=1}^{M_r} (v''_{s,r} - v'_{s,r}) k_r \sum_{p=1}^{M_s} H_{p,l} \, v'_{p,r} \, N_p^{-1} \prod_{k=1}^{M_s} N_k^{v'_{k,r}} \tag{A6}
$$

The initial conditions are $H_{s,l} = \delta_{s,l}$ at position $x = 0$.

Appendix B: Optimization Approach

The model regression is based on minimizing the residual

$$
\mathcal{R}(\mathbf{y}, \mathbf{k}) = \sum_{l=1}^{M} \frac{(y_l - f_l(\mathbf{k}))^2}{2\sigma_l^2} \tag{B1}
$$

with respect to $\mathbf{k}$, the vector of parameters $k_1, \ldots, k_L$. The elements $y_l, l = 1, \ldots, M$ of vector $\mathbf{y}$ denote experimentally found species densities and $f_l(\mathbf{k})$ the corresponding result obtained by integrating the rate equations. The variances σ_l^2 denote empirical noise or arbitrarily chosen inverse weights for the experimental data. The deviation of the observable particle densities y_l from the model predictions f_l for different values of the plasma power P is considered here. To obtain the model data f_l, the rate equations for a given plasma power are integrated up to a fixed point x_*. In terms of Bayesian statistics, the minimization of residual $\mathcal{R}$ is equivalent to the maximization of the Gaussian likelihood $\mathcal{L}$, given by

$$
\mathcal{L}(\mathbf{y}|\mathbf{k}) = \frac{\exp\left\{ -\sum_{l=1}^{M} \frac{(y_l - f_l(\mathbf{k}))^2}{2\sigma_l^2} \right\}}{\prod_{l=1}^{M} \left(2\pi\sigma_l^2\right)^{1/2}} \tag{B2}
$$

Therefore, the best-fit parameters $\hat{\mathbf{k}}(\mathbf{y})$ for the data given are the Maximum Likelihood Estimate (MLE) for this particular choice for the likelihood, formally written as

$$
\hat{\mathbf{k}}(\mathbf{y}) = \underset{\mathbf{k}}{\operatorname{argmax}} \; \mathcal{L}(\mathbf{y}|\mathbf{k}) \tag{B3}
$$

The method of choice for this optimization problem is a genetic algorithm where we use an approach successfully employed in previous work and documented there [12]. Further references to texts on genetic algorithms can also be found there. The sensitivity matrix is defined by

$$\mathbf{S(k)} = \frac{1}{M} \sum_{l=1}^{M} \frac{\partial \ln f_l(\mathbf{k})}{\partial \mathbf{k}} \frac{\partial \ln f_l(\mathbf{k})}{\partial \mathbf{k}} \tag{B4}$$

It is strongly related to the Fisher information $\mathbf{F(k)}$, which is generally defined by

$$\mathbf{F(k)} = \int \frac{\partial \ln \mathcal{L}(\mathbf{y}|\mathbf{k})}{\partial \mathbf{k}} \frac{\partial \ln \mathcal{L}(\mathbf{y}|\mathbf{k})}{\partial \mathbf{k}} \mathcal{L}(\mathbf{y}|\mathbf{k}) \, d\mathbf{y} \tag{B5}$$

In our special case of a Gaussian likelihood $\mathbf{F(k)}$ can be written as

$$\mathbf{F(k)} = \sum_{l=1}^{M} \sigma_l^{-2} \frac{\partial f_l(\mathbf{k})}{\partial \mathbf{k}} \frac{\partial f_l(\mathbf{k})}{\partial \mathbf{k}} \tag{B6}$$

For the reaction kinetic models considered here, the calculation of the derivatives $\partial f_l / \partial k_i$ is equivalent to the determination of the derivatives of the particle species N_s with respect to the rate coefficients k_i. This can be done using the "direct method" [16] simultaneously calculating the particle densities f_l. The relevant formulas are listed in Appendix 9. The usefulness of the sensitivity matrix for statistical analysis of the identifiability of model parameters and the calculation of confidences via the inverse of the Fisher information (Cramér–Rao bound) are richly documented in the literature (see, e. g. , [17–22]). A special feature of the reaction kinetic models is that the rate coefficients are all positive definite. Introducing $\xi_i = \ln k_i$ allows to define

$$\mathbf{S(\xi)} = \frac{1}{M} \sum_{l=1}^{M} \frac{\partial \ln f_l(\xi)}{\partial \xi} \frac{\partial \ln f_l(\xi)}{\partial \xi} \tag{B7}$$

where

$$\frac{\partial \ln f_l(\xi)}{\partial \xi_i} = k_i \frac{\partial \ln f_l(\mathbf{k})}{\partial k_i} \tag{B8}$$

Similarly, a Fisher information $\mathbf{F(\xi)}$ can be introduced as

$$\mathbf{F(\xi)} = \sum_{l=1}^{M} \sigma_l^{-2} \frac{\partial f_l(\xi)}{\partial \xi} \frac{\partial f_l(\xi)}{\partial \xi} \tag{B9}$$

We want to note that the choice of logarithmic parameters ξ is also used in the optimization with the genetic algorithm to automatically guarantee that the rate coefficients are non-negative.

Using the Fisher information $\mathbf{F(\xi)}$ confidence intervals for optimal rate coefficients $\hat{k}_i$ can be computed via

$$\hat{k}_i e^{-1.96 \sqrt{\hat{C}_{ii}}} \leq \hat{k}_i \leq \hat{k}_i e^{+1.96 \sqrt{\hat{C}_{ii}}} \tag{B10}$$

where $\hat{C}_{ii}$ is a diagonal element of the inverse of the Fisher information

$$\hat{\mathbf{C}} = \mathbf{F}^{-1}(\hat{\xi}) \tag{B11}$$

This estimate for the covariance matrix $\hat{\mathbf{C}}$ is based on the Cramér–Rao bound giving a lower limit for the variances of the regression parameters [18]. Therefore, the confidence intervals do not give any information on the "true" values of some physical numbers for the model

parameters, but they give an impression of how the regression can obtain sharp certain parameters compared to the others.

Appendix C: Sensitivity Matrix and Identifiability

To analyze the quality of a model, the sensitivity matrix defined by Eq. B7 is considered for the best fit parameter $\hat{\xi}$ and decomposed via Singular Value Decomposition

$$\mathbf{S}(\hat{\xi}) = \mathbf{U} \cdot \Sigma \cdot \mathbf{U}^{\mathrm{T}} \tag{C1}$$

The components of $\mathbf{U}$ are

$$U_{ij} = \mathbf{e}_i \cdot \mathbf{u}_j \tag{C2}$$

where the vectors $\mathbf{u}_j$ are the normalized eigenvectors of $\mathbf{S}(\hat{\xi})$, corresponding to the singular values σ_j, $j = 1, \dots, L$ in descending order $\sigma_1 \geq \sigma_2 \geq \dots \geq \sigma_L \geq 0$. These eigenvalues form the diagonal of the matrix Σ. Here L denotes the number of model parameters and $\mathbf{e}_i$, $i = 1, \dots, L$ are the base vectors in the cartesian ξ-parameter space. Introducing the coordinates (new model parameters) ϕ as

$$\phi = \mathbf{U}^{\mathrm{T}} \cdot \xi \quad , \quad \xi = \mathbf{U} \cdot \phi \tag{C3}$$

gives for the sensitivities

$$\frac{\partial \ln f_l}{\partial \phi} = \mathbf{U}^{\mathrm{T}} \cdot \frac{\partial \ln f_l}{\partial \xi} \quad , \quad \frac{\partial \ln f_l}{\partial \xi} = \mathbf{U} \cdot \frac{\partial \ln f_l}{\partial \phi} \tag{C4}$$

Thus, for a particular eigenvector $\mathbf{u}_i$

$$\sum_{l=1}^{M} \mathbf{u}_i \cdot \frac{\partial \ln f_l}{\partial \hat{\xi}} \frac{\partial \ln f_l}{\partial \hat{\xi}} \cdot \mathbf{u}_i = \sum_{l=1}^{M} \left(\frac{\partial \ln f_l}{\partial \hat{\phi}_{\mathbf{i}}} \right)^2 = M \sigma_i \tag{C5}$$

The notation $\partial \ln f_l / \partial \hat{\xi}$ means the derivative $\partial \ln f_l / \partial \xi$ taken at the optimal parameters $\hat{\xi}$. Consequently, if the singular value σ_i is zero all f_l (and the related likelihood considered above) do not change in the direction of the corresponding coordinate ϕ_i. In other words, such a coordinate can not be identified because it does not affect the likelihood of the parameter optimization problem. Therefore, if the rank of $\mathbf{S}(\hat{\xi})$ is less than L, it can be concluded that the model has more parameters than justified by the data. This could be caused by the fact that the likelihood is independent of one or more parameters, that the data are insufficient or that there is some redundancy in the sensitivity matrix. The sensitivity matrix is diagonal in the parameters ϕ, and according to Eq. C1

$$\mathbf{S}(\hat{\phi}) = \frac{1}{M} \sum_{l=1}^{M} \frac{\partial \ln f_l}{\partial \hat{\phi}} \frac{\partial \ln f_l}{\partial \hat{\phi}} = \Sigma \tag{C6}$$

An important point in using the logarithmic derivatives $\partial \ln f_l / \partial \xi$ in the definition of $\mathbf{S}(\hat{\xi})$ is that the new parameters ϕ can be expressed as

$$\phi_i = \sum_{j=1}^{L} U_{ji} \xi_j = \ln \left(\prod_{j=1}^{L} k_j^{U_{ji}} \right) \tag{C7}$$

and it is useful to define a further set of parameters $\zeta_i = e^{\phi_i}$. The relations between the parameter set $\mathbf{k}$ and the new set ζ are thus

$$\zeta_i = \prod_{j=1}^{L} k_j^{U_{ji}} \quad , \quad k_i = \prod_{j=1}^{L} \zeta_j^{U_{ij}} \tag{C8}$$

Assuming now that $\text{rank}(\mathbf{S}) = r < L$ it follows that the parameters ζ_j with $j = r+1, \ldots, L$ (corresponding to the zero eigenvalues) are irrelevant. This means—and this is one of the main results of this section-, if we multiply the coordinates ζ_j with $j = r+1, \ldots, L$, each by a factor $a_j > 1$, the resulting parameters k_i give as good a regression as the best-fit parameters $\hat{k}_i$. In other words, the regression with parameters k_i is equivalent to the regression with $\hat{k}_i$, if

$$k_i = \hat{k}_i \prod_{j=r+1}^{L} a_j^{U_{ij}} \tag{C9}$$

Because of this arbitrariness, the parameters ζ_j with $j = r+1, \ldots, L$ can also be neglected (i.e. fixed to $\hat{\zeta}_j$) from the expressions for the k_i, and the following reduction yields a re-parametrization

$$k_i = \prod_{j=1}^{r} \zeta_j^{U_{ij}} \tag{C10}$$

Inserting these expressions for the parameters k_i, $i = 1, \ldots, L$ into the original rate equations equations reduce the number of regression parameters from L to r. The same transformations can also be applied to the known Fisher matrix $\mathbf{F}(\hat{\xi})$ to obtain the uncertainties of the new coordinates. This follows from

$$\mathbf{F}(\hat{\phi}) = \sum_{l=1}^{M} \sigma_l^{-2} \frac{\partial f_l}{\partial \hat{\phi}} \frac{\partial f_l}{\partial \hat{\phi}} = \mathbf{U}^{\mathrm{T}} \cdot \mathbf{F}(\hat{\xi}) \cdot \mathbf{U} \tag{C11}$$

The irrelevant coordinates ϕ_i, $i = r+1, \ldots, L$ give only zero entries in the Fisher matrix

$$\mathbf{F}(\hat{\phi}) = \begin{pmatrix} \tilde{\mathbf{F}}(\hat{\phi}) & \mathbf{0} \\ \mathbf{0} & \mathbf{0} \end{pmatrix} \tag{C12}$$

Therefore, it is sufficient to consider the sub-matrix $\tilde{\mathbf{F}}(\hat{\phi}) \in \mathbb{R}^{r \times r}$. This sub-matrix is invertible and the inverse of $\tilde{\mathbf{F}}(\hat{\phi})$ gives the lower bound (Cramér-Rao bound) for the covariance matrix $\tilde{\mathbf{C}}(\hat{\phi})$ of the relevant parameters $\hat{\phi}_i$, $i = 1, \ldots, r$. Practically, the sub-matrix $\tilde{\mathbf{F}}(\hat{\phi})$ is given by

$$\tilde{\mathbf{F}}(\hat{\phi}) = \mathbf{W}^{\mathrm{T}} \cdot \mathbf{F}(\hat{\xi}) \cdot \mathbf{W} \tag{C13}$$

where the matrix $\mathbf{W} \in \mathbb{R}^{L \times r}$ is a sub-matrix of $\mathbf{U}$

$$W_{ij} = U_{ij} \quad , \quad i = 1, \ldots, L \quad j = 1, \ldots, r \tag{C14}$$

Neglecting the eigenvectors corresponding to (almost) zero eigenvalues is equivalent to regularization and subsequent reduction of the Fisher matrix.

References

1. Stewig C, Chauvet L, von Keudell A (2023) Impact of catalysis on n-butane oxidation in an rf atmospheric pressure plasma. Plasma Sources Sci Technol 32:105006

2. Schücke L, Gembus J-L, Peters N, Kogelheide F, Nguyen-Smith RT, Gibson AR, Schulze J, Muhler M, Awakowicz P (2020) Conversion of volatile organic compounds in a twin surface dielectric barrier discharge. Plasma Sources Sci Technol 29(11):114003

3. Jin-Oh J, Trinh HQ, Kim SH, Mok YS (2016) Simultaneous removal of hydrocarbon and CO using a nonthermal plasma-catalytic hybrid reactor system. Chem Eng J 299:93–103

4. Urbanietz T, Stewig C, Böke M, von Keudell A (2021) Oxygen removal from a hydrocarbon containing gas stream by plasma catalysis. Plasma Chem Plasma Process 41(2):619–642

5. Wandell RJ, Locke BR (2017) Hydrocarbon processing by plasma. Springer, Cham, pp 1163–1182

6. Böddecker A, Bodnar A, Schücke L, Giesekus J, Wenselau K, Nguyen-Smith RT, Oppotsch T, Oberste-Beulmann C, Muhler M, Gibson AR, Awakowicz P (2022) A scalable twin surface dielectric barrier discharge system for pollution remediation at high gas flow rates. React Chem Eng 7:2348–2358

7. Peters N, Schücke L, Ollegott K, Oberste-Beulmann C, Awakowicz P, Muhler M (2021) Catalyst-enhanced plasma oxidation of n-butane over MnO_2 in a temperature-controlled twin surface dielectric barrier discharge reactor. Plasma Process Polym 18:202000127

8. Bogaerts A, Neyts EC (2018) Plasma technology: an emerging technology for energy storage. ACS Energy Lett 3(4):1013–1027

9. Bogaerts A, Tu X, Whitehead JC, Centi G, Lefferts L, Guaitella O, Azzolina-Jury F, Kim H-H, Murphy AB, Schneider WF, Nozaki T, Hicks JC, Rousseau A, Thevenet F, Khacef A, Carreon M (2020) The 2020 plasma catalysis roadmap. J Phys D Appl Phys 53(44):443001

10. Stewig C, Schüttler S, Urbanietz T, Böke M, von Keudell A (2020) Excitation and dissociation of CO_2 heavily diluted in noble gas atmospheric pressure plasma. J Phys D Appl Phys 53(12):125205

11. Stewig C, Urbanietz T, Chauvet L, Böke M, von Keudell A (2021) Dedicated setup to isolate plasma catalysis mechanisms. J Phys D 54:134005

12. Reiser D, Urbanietz T, von Keudell A (2020) Determining chemical reaction systems in plasma catalytic conversion of hydrocarbons using genetic algorithms. Plasma Chem Plasma Process 41:793

13. Chen G, Britun N, Godfroid T, Georgieva V, Snyders R, Delplancke-Ogletree M-P (2017) An overview of CO_2 conversion in a microwave discharge: the role of plasma-catalysis. J Phys D Appl Phys 50(8):084001

14. Koop J, Deutschmann O (2009) Detailed surface reaction mechanism for Pt-catalyzed abatement of automotive exhaust gases. Appl Catal B 91(1):47–58

15. Deutschmann O, Tischer S, Kleditzsch S, Janardhanan V, Correa C, Chatterjee D, Mladenov N, Minh HD, Karadeniz H, Hettel M, Menon V, Banerjee A, Gossler H, Shirsath A, Daymo E (2022) DETCHEM. https://www.detchem.com

16. Turányi T (1990) Sensitivity analysis of complex kinetic systems. Tools and applications. J Math Chem 5(3):203–248

17. Ly A, Marsman M, Verhagen J, Grasman RPPP, Wagenmakers E-J (2017) A tutorial on fisher information. J Math Psychol 80:40–55

18. Reimer J, Schuerch M, Slawig T (2015) Optimization of model parameters and experimental designs with the optimal experimental design toolbox (v1.0) exemplified by sedimentation in salt marshes. Geosci Model Dev 8(3):791–804

19. Lindsay BG, Yao W (2012) Fisher information matrix: a tool for dimension reduction, projection pursuit, independent component analysis, and more. Can J Stat 40(4):712–730

20. Cintrón-Arias A, Banks HT, Capaldi A, Lloyd AL (2009) A sensitivity matrix based methodology for inverse problem formulation. J Inverse Ill-Posed Probl 17(6):545–564

21. Vajda S, Valko P, Turányi T (1985) Principal component analysis of kinetic models. Int J Chem Kinet 17(1):55–81

22. Mosbach S, Hong JH, Brownbridge GPE, Kraft M, Gudiyella S, Brezinsky K (2014) Bayesian error propagation for a kinetic model of n-propylbenzene oxidation in a shock tube. Int J Chem Kinet 46(7):389–404